The Role of Trigger Thresholds
in Experimental Design and Physics Outcomes in High Energy Neutrino Astronomy

Brian A. Clark

PhD Candidacy Written Examination
Department of Physics
The Ohio State University

Candidacy Committee:
Prof. Amy Connolly, Chair
Prof. James Beatty
Prof. John Beacom
Prof. Lynn Van Woerkom

June 28, 2016

Contents

1 Introduction

Neutrinos represent a unique observational window on the universe. As chargeless, weakly interacting particles, neutrinos serve as one of the only astrophysical messengers at cosmological distances (> 50 Mpc). Hadrons are destroyed by interactions with the Cosmic Microwave Background (CMB) and photons pair annihilate with the CMB and Extragalactic Background Light (EBL). Detection at earth is challenging due to low incident fluxes and low cross sections for interaction; we will quantify this in the next section.

A potential observation channel is to look for the electromagnetic signature of a neutrino's rare interaction with matter when they arrive at Earth. If the interaction takes place in a dense dielectric medium, the relativistic by-products can emit distinctive optical and radio Cherenkov light. Experiments look for this light in large naturally occurring targets like the Antarctic ice sheet. Unfortunately, these signals have formidable astrophysical, anthropogenic ("human made"), and thermal backgrounds. To solve this problem, experiments develop triggers whose task is efficiently differentiating signal, when it occurs, from the background noise. If the trigger is poorly designed, or its thresholds optimized incorrectly, the experiment could have its hardware limitations (data storage space, digitizer buffers, etc.) consumed by physically meaningless background and fail to record signals of interest. Precisely how well a trigger must do its job depends primarily on the limitations of the hardware. In this work, we will review a selection of high-energy neutrino experiments, and discuss how their triggers and trigger thresholds impact their physics reach. We will discuss the IceCube, Antarctic Impulsive Transient Antenna (ANITA), and Askaryan Radio Array (ARA) experiments, review a general procedure for optimizing a trigger, and conclude with a discussion of a new proposed experiment, the Greenland Neutrino Observatory (GNO).

2 Target Physics

The physics targets of the experiments set their scale, as the overall size of the detector directly affects the energy range to which the experiments are sensitive. As detailed in [1], IceCube's principal physics target is the astrophysical neutrino flux between a 1 TeV and several PeV, where there are neutrinos expected from systems such as Gamma Ray Bursts (GRBs), Supernovae, etc. For example, Waxman and Bahcall [2] suggest that a km^2 detector would find $\sim$ 10-100 events of

energy 100 TeV from GRBs. So IceCube, with its instrumented volume of 1 km^3, is well suited to find fluxes in this energy range.

ANITA and ARA are built to detect the rarer EeV neutrino flux and the experiments are commensurately larger. The experiments are interested in EeV neutrinos very broadly, whatever their sources may be, though a primary physics target is discovery of the elusive Berezinsky-Zatsepin flux. It is an experimental fact that the cosmic ray spectrum is attenuated at $E^{19.5}$ eV, at the threshold of the interaction $p+\gamma \rightarrow\ n+\pi^+$ with $E_\gamma \approx 3\times10^{-4}$ eV, or roughly a CMB photon; this interaction is known as the Greisen, Zatsepin, and Kuzmin (GZK) cutoff [3, 4]. The pions are expected to decay into a μ^+ and ν_μ, and the muon further through $\mu^+ \rightarrow e^+ + \nu_e + \bar{\nu}_\mu$; this GZK associated neutrino production is known as the Berezinsky and Zatsepin (BZ) flux [5]. A model for this flux by Ahlers *et. al.* [6] predicts EeV BZ neutrinos should *arrive* at Earth with an incident flux of $\sim 10\,\nu/\mathrm{km}^2/\mathrm{yr}/\mathrm{sr}$, but the low cross section of $\sigma = 10^{-32}\mathrm{cm}^2$ [7] gives an *interaction* rate in ice ($\rho = 0.9\mathrm{g}/\mathrm{cm}^3$) of $< 3\times10^{-3}\nu/\mathrm{km}^3/\mathrm{yr}/\mathrm{sr}$. With enormous apertures, ANITA and ARA are engineered to find this, and other, ultra-high energy neutrino fluxes. ANITA observes an area of $10^6\,\mathrm{km}^2$ and is designed to monitor the $10^{18}-10^{21+}$ eV energy range, while ARA with an observing area of $10^2\,\mathrm{km}^2$ probes the $10^{16}-10^{19}$ eV energy range.

The detector's ability to access this target physics, its *sensitivity*, is dependent on high quality trigger design. Sensitivity is expressed through energy threshold and aperture for event collection. The aperture will be encoded in either the effective volume or effective area of the detectors, since flux estimates are estimated as incident neutrinos-per-area and interaction rates are estimated in neutrino interactions-per-volume. In the literature, the effective-area or effective-volume is often computed in Monte Carlo simulations by forcing the interaction of a certain number of neutrinos N_{int} inside a hypothetical detector volume V_{det}, finding the number of neutrinos that are detected at the end of the signal chain N_{det}, and taking the ratio between the two [8, 9]:

$$A_{eff}(E_\nu,\theta) = \frac{N_{det}(E_\nu,\theta)}{N_{int}} \times A_{int} \iff V_{eff} = \frac{N_{det}(E_\nu,\theta)}{N_{int}} \times V_{int} \tag{1}$$

A_{eff} is the effective area, and is related to the effective volume in the thin-target approximation [10] by $V_{eff} = L_{int}A_{eff}$ where L_{int} is the interaction length of the particle. The dependence on the efficiency, and therefore the trigger, is encoded in N_{det}.

3 Review of Select HE Neutrino Experiments

3.1 The Optical Cherenkov Experiment IceCube

Neutrino-nucleon interactions produce daughter particles that can be detected by their Cherenkov radiation. A neutrino can interact with matter through a "charged-current" (CC) $W^{\pm}$-vector-boson mediated interaction or "neutral-current" (NC) Z^0-vector-boson mediated interaction. The CC interaction is $\nu_\ell + N \rightarrow \ell + X$, where N is a nucleon (proton or neutron) and X is an outgoing hadronic shower; the lepton ℓ can induce an electromagnetic (EM) shower. The NC interaction is $\nu + N \rightarrow \nu + N^*$, where the recoiling nucleon N^* induces a hadronic shower. The outgoing charged particles are ultra-relativistic ($\beta \approx 1$), and so if the interaction occurs in a medium other than air/-vacuum, the particle is moving faster than the speed of light in that medium, and emits Cherenkov radiation [11]. This radiation is dominated by blue light and near-UV light as the intensity of the light goes as $1/\lambda^2$ [12]. The light is emitted preferentially in a cone with an opening angle termed the Cherenkov angle θ_c, defined by the speed of the particle and the index of refraction ($\cos(\theta_c) = 1/n\beta$), and is $\sim 57^\circ$ in glacial ice ($n = 1.78$).

The IceCube experiment seeks to observe this optical Cherenkov effect in the clear glacial ice of the South Pole. The experiment buries photomultiplier tubes (PMTs), sensitive to blue and UV light (300-650nm) [13] deep into the Antarctic ice. Completed in 2011, there are 5160 PMTs placed in 10-inch pressured spherical vessels nicknamed digital optical modules, or DOMs. The DOMs are deployed on vertical strings: 60 DOMs per string, 17m between DOMs, across 86 strings, with 125m of spacing between the strings [12]. The DOMs are placed at a depth of 1500-2500 meters, where the properties of the deep glacial ice give scattering lengths of ~ 20 m [14], and extinction lengths of over 100 m [15]. The total instrumented volume of the IceCube detector is 1 km^3.

IceCube has two primary backgrounds: the dark rate of the PMTs and the flux of atmospheric neutrinos and muons. The Dark Rate of a PMT is defined as the rate at which the PMT will produce a signal in the absence of externally applied light. IceCube's dark rate is suppressed by the cold temperatures of the DOMs (-32°C at the uppermost DOM and -9°C at the lowest), as well as by the fact that the DOM is in very dark ice, being buried > 7 extinction lengths beneath the surface. The observed dark rate for the IceCube PMT is 500 Hz. The flux of atmospheric neutrinos and muons arises from the decay of pions and kaons produced by the collision of cosmic

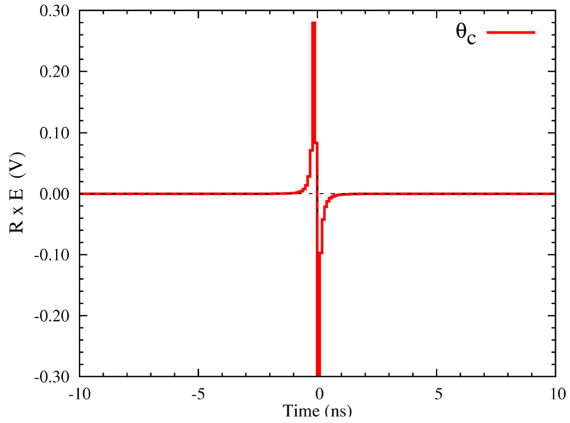

Figure 1: A sample electric field from a simulated 1 PeV electron-induced shower viewed at the Cherenkov angle; figure from [20].

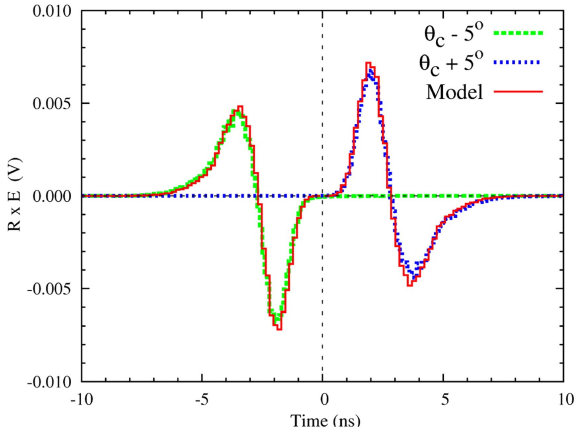

Figure 2: A sample electric field from a simulated 1 PeV electron-induced shower viewed off the Cherenkov angle. Figure from [20]. "Model" refers to the work in [20].

rays with the atmosphere [16]. The neutrinos can either interact in the atmosphere or in the ice; both produce signals similar to those made by astrophysical neutrinos in the detector.

3.2 The Radio Cherenkov (Askaryan) Experiments ANITA and ARA

The daughter particles of neutrino-nucleon interactions also produce observable radio Cherenkov emission, interchangeably referred to as Askaryan radiation. The EM/hadronic showers develop $\sim 20\%$ negative charge asymmetries because positrons in the shower are destroyed via pair annihilation but photons and electrons ionize the medium through Compton scattering and the photoelectric effect. For wavelengths greater than the size of the shower ($\sim$ 10 cm in ice), the waves add *constructively*, producing a broadband (200 MHz-1.2 GHz) radio pulse [17]. The signal is emitted at the same Cherenkov angle as for optical light, and lasts anywhere from 100 ps to several ns, depending on if the pulse is viewed "on-cone" (at θ_c exactly) or "off-cone" [18, 19]. The Cherenkov cone is polarized, with the polarization vector perpendicular to the line-of-sight to the shower. The profile of the pulse is very narrow with a width of less than 6°, and it both broadens in time and loses its high frequency content as the signal is viewed increasingly off-cone. Deterioration of both high frequency content and overall signal magnitude is caused by the decoherence of the shorter wavelengths. In Antarctic ice, this radio wave can travel for hundreds of meters minimally attenuated, with an average attenuation length of 690 meters at 300 MHz[8].

The Antarctic Impulsive Transient Antenna, or ANITA experiment, seeks to observe the radio Cherenkov light from neutrino induced showers in the Antarctic ice sheet. ANITA is an array of highly directional, dual-polarized, broadband (200-1200 MHz) horn antennas that is flown by a NASA long duration balloon at an altitude of 40 kilometers above the Antarctic Ice. The antennas are arranged in stacked rings to achieve full azimuthal coverage of the Antarctic continent, and are canted downward 10° to preferentially observe ice, not sky. There have been three ANITA campaigns (ANITA 1, 2, 3), with a fourth planned for Austral summer 2016. The ANITA experiment can view over a million square kilometers of ice [21] and is designed to be sensitive to neutrinos above an EeV in energy. ANITA is primarily sensitive to "earth-skimming" neutrinos. Such neutrinos enter the Antarctic ice after traversing very little of the earth's mantle and crust; the earth becomes opaque to neutrinos above a PeV [7], so entering from steeper elevation angles results in absorption [22]. Because the neutrinos are earth-skimming, and enter almost horizontally, ANITA is likely to only detect the top of the Cherenkov cone, which would be vertically polarized.

The Askaryan Radio Array, or ARA experiment, also looks for Askaryan pulses in Antarctic ice, but instead of observing the ice from a high altitude, it relies on detectors buried in the medium as an *in-situ* experiment. The proposed ARA experiment is an array of 37 neutrino detecting stations; there are currently 3 of the 37 installed. Each station consists of 16 omni-directional antennas (eight vertically polarized, eight horizontally polarized) deployed in a cubical lattice. The antennas are buried 200 meters deep inside vertical holes. There are four antennas per hole, two of each polarization. The antennas have broad frequency coverage (200-850 MHz), and the full 37-station array will instrument roughly 100 square-kilometers of ice, and seeks to measure neutrinos between $10^{16} - 10^{19}$ eV. Like ANITA, the neutrinos of interest are highly earth attenuated, so ARA is also primarily sensitive to earth-skimming neutrinos.

ANITA and ARA's primary background at the trigger level is thermal noise, specifically the blackbody radio emission from the Antarctic ice [21]. Additional backgrounds include continuous wave (CW) emission from human sources like radio and satellite communication [8], as well as impulsive electromagnetic interference (EMI), such as sparks from lighters or static discharge on the arid continent [23].

4 Triggering Schemes

Triggering is a decision made by a detector's Data Acquisition System (or DAQ) about whether to record a piece of information. Triggers are important because constant digitization and storage of signal is often impossible for storage and power constraint reasons. ANITA and ARA must operate on less than 1 kW of power total, which limits their ability to run dozens of 5-10 Watt digitizers constantly. Continuously sampling and storing a 3 GHz signal, with each 256 voltage samples requiring 36 kB of space, would generate over 150 giga-bytes of data *per second* [21]. Experiments design trigger schemes to distinguish between the common backgrounds, and the rare astrophysical signals; this reduces the volume of data to be recorded and studied.

4.1 IceCube and its Trigger

The IceCube triggering scheme is two fold and is designed to suppress the PMT dark rate and maximize sensitivity to through-going track-like muon events. The trigger must decrease the individual DOM trigger from the 500 Hz dark rate to less than 90 Hz. This maximum is set by the bandwidth with which the data can be read out from the DOMs to the central data storage center at the Antarctic surface. This can be accomplished at a speed of approximately 900 kB/s per string [15]. If each DOM waveform requires 170 bytes, and there are 60 DOMs per string, the maximum trigger rate allowed per DOM is < 88 Hz [1]. This estimate does not account for housekeeping data which could increase the size of each triggered event.

In the trigger scheme, IceCube first requires a PMT anode pulse above 0.25 single photoelectron height [15]. Because the measured signal of a single incident photon produces a 10 mV pulse of 5 ns duration into the 43 Ω impedance of the IceCube DAQ [24], this is the equivalent of requiring the output voltage of the PMT to go above 2.5mV. Secondly, IceCube requires a simple multiplicity trigger (SMT), which demands that a tunable number of DOMs in the array attain a "local coincidence" (LC) trigger [15]. A LC-trigger is obtained when a DOM has a nearest-neighbor or next-to-nearest neighbor DOM trip the voltage requirement in a 2 μs trigger window. Typically, the SMT trigger is set to either 5 or 8 DOMs, and as low as 3 DOMs for DeepCore. DeepCore is a densely spaced infill array of the larger bulk detector, where DOM spacing is reduced to 10 meters [25]. The LC trigger rate for a single DOM is 10 Hz.

IceCube performs all background suppression with this LC trigger; the PMT threshold trigger is set so low that it offers essentially no discriminatory power [13]. For a DOM dark rate $r = 500$Hz and a LC window $\tau = 2\,\mu$s, the rate at which a DOM and at least one of its 4 neighbors triggers due to background coincidences is $4r^2\tau = 2$ Hz [26], close to the observed rate mentioned above. This LC trigger condition cuts down the number of random DOM-related background events by two orders of magnitude and achieves the rate suppression necessary for the hardware trigger maximum. We emphasize that this trigger does not lose physics information. An isolated DOM trigger (no LC condition met) is 100 times more likely to be background than physics signal [1], and further, simulations show (fig 3a) that even the lowest energy muons of interest at a few GeV typically leave tracks that trigger at least 10 DOMs.

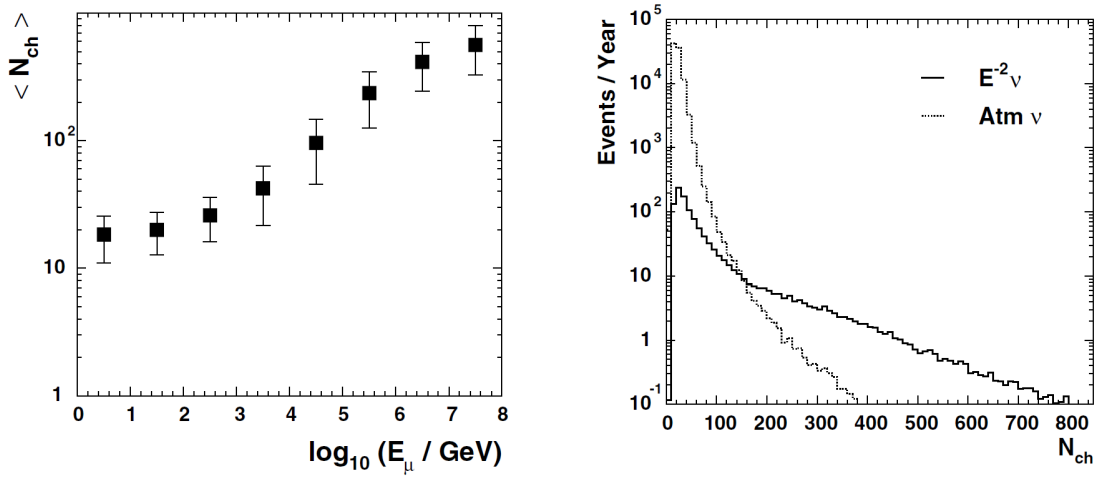

Figure 3: (a, left): Simulated average number of DOMs triggered as a function of muon energy. (b, right): Simulated number of DOMs triggered for an E^{-2} cosmogenic neutrino flux and an atmospheric background. Figures from [27].

The background rate for atmospheric neutrinos and muons is estimated by the collaboration via Monte Carlo simulations to be roughly 1.7 kHz [27] for muons above a GeV. The simulation estimates this full array trigger rate for a five-fold local coincidence trigger in the presence of an atmospheric neutrino background in addition to a cosmogenic neutrino flux. This roughly agrees with the 2008 update from IceCube which claims that of an experimentally observed trigger rate of 1.4 kHz on the half-finished array, roughly 1 kHz are atmospheric muons [24] (the remaining 400 Hz were attributed to other sources, including the IceTop cosmic ray detector). This 1.4 kHz translates to triggering rates for individuals DOMs of less than a Hz, well under the hardware maximum.

4.2 ARA and its Trigger

The ARA experiment likewise has a two-stage trigger; the first stage tests for impulsiveness, and the second stage for reconstructability. Both triggers combined must produce a global trigger rate of approximately 5 Hz, which is set by hardware limitations. For every triggered event, ARA incurs a digitization deadtime (1 ms) and write-to-disk deadtime (20 ms) [28]; this limits the maximum trigger rate to < 48 Hz. However, the experiment must also store all data locally for an entire calendar year. If an event is 36 kB in size (not atypical of ARA or ANITA) [21], the small on-board hard drive of 5.4 TB can store 1.5×10^8 events, which gives rise to the 5 Hz storable event rate (5.4 TB/3.6 kB/# seconds per year).

The first stage of the trigger requires that for a single antenna, the integrated *power* in a several nano-second time window must exceed a threshold level set by the thermal background. This is termed an "L0 trigger". The physical motivation of this trigger is the "pulse" nature of the Askaryan signal, which suggests that all of the detectable power should be located within a several-ns time window. Power integration is accomplished by passing the waveform through a diode whose output voltage is proportional to the input squared, and therefore proportional to power. The trigger fires when the diode output goes above some threshold; the threshold is usually defined as a multiple of the mean of the output. An example of a simulated diode output is given in figure 4 where $F(t)$ should be regarded as the diode output and $< F(t) >$ should be regarded as its mean. The mean noise power, which we call P_{rms} and is labeled $< F(t) >$ in the figure, is given by the power dissipated by pure thermal noise in a resistor of impedance Z. $P_{rms} = V_{rms}^2/Z$ with

$$V_{rms} = \sqrt{4k_B T \Delta f Z} \tag{2}$$

where k_B is Boltzmann's constant. For the ARA system, with $T = 325$ K and $\Delta f = 650$ MHz [29] the $V_{rms} = 24\mu$V. The rate R at which the thermal noise background with mean power P_{rms} exceeds the threshold P_{th} over some bandwidth Δf is given by [30]

$$R(P_{rms} > P_{th}) = \Delta f \exp\left(\frac{-P_{th}}{P_{rms}}\right) \tag{3}$$

$R(P_{rms} > P_{th}) = R_{L0}$ is termed the single-channel trigger rate or SCTR. *Therefore, the rate at*

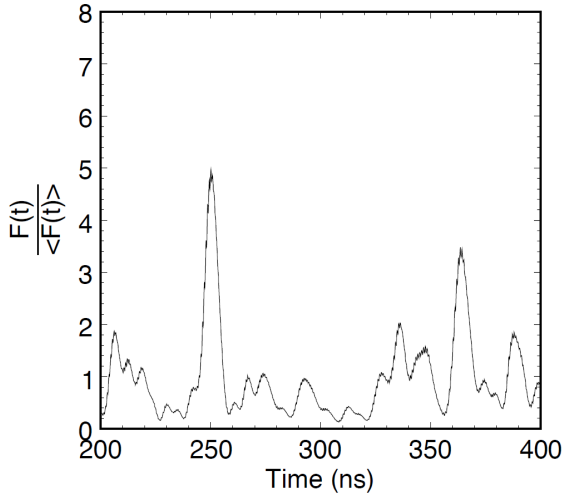

Figure 4: A sample normalized diode output as a function of time. $F(t)$ models the diode output, and $< F(t) >$ represents its mean. Figure from [30].

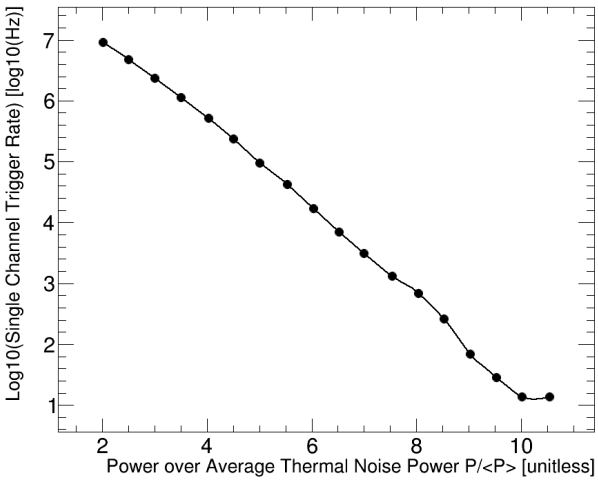

Figure 5: The single-channel trigger rate (SCTR) from simulation for stations 1-3 as a function of noise sigma. Figure from data in [31].

which a single channel triggers is exponentially dependent upon the chosen trigger threshold. A plot of the SCTR from simulations [31] is given in figure 5. ARA currently triggers on 5 to 6 times the mean thermal noise power. At this threshold level, the SCTR for ARA from simulation can be read off figure 5 as $\sim 10^4$ Hz. In the actual stations, the threshold P_{th} is actively monitored on a per-antenna basis and modified every 1 Hz to hold the SCTR constant about the $\sim 10^4$ Hz rate.

The second trigger condition for ARA is a "multiplicity trigger," which demands that 3/8 antennas of a given polarization must have an L0 trigger in a 170 ns window; this is termed an "L1" trigger. The global trigger rate R_{global} [8] can be given by the probability that k out of n channels trigger in a time τ, where each channel triggers with the rate r given in equation 3:

$$R_{global} = 2nrP(k:n) = 2\frac{n!}{k!(n-k)!}r^k\tau^{k-1} \tag{4}$$

The factor of 2 accounts for the fact that ARA can trigger on vertically or horizontally polarized signals. If a global trigger is issued, the entire array is read out for 400 ns centered on the first triggered antenna [32]. By equation 4, we expect $R_{global} = 2 \cdot \frac{8!}{3!\cdot 5!} r_{L0}^3 \tau_{L1}^2$ which for $r_{L0} = 10^4$ Hz and $\tau_{L1} = 1$ 170 ns, we find $R_{global} = 3.2$ Hz. The operating rate is approximately 5 Hz, in good agreement with our predictions. The triggering parameters are physically motivated: 170 ns

allows a light signal to traverse the longest antenna baseline in the array (a 52 meter length across the diagonal of the cube) and 3/8 antennas will uniquely define a plane of arrival for the signal wave. Requiring 3/8 antennas thus incorporates analysis level information at the trigger level. The decision to do so is a matter of preference, as analysis constraints evolve and improve with time. Either way, such considerations highlight that the trigger thresholds are not only used for background reduction, but also have direct ties to the experimental design, and underscores why care must be taken to determine and optimize the triggers.

By imposing a 3/8 multiplicity trigger, equation 4 conveys that the global trigger rate depends *at least* cubically on the SCTR, which in turn depends exponentially on the threshold. So $R_{global} \propto e^{-3P_{th}}$. If the threshold is lowered, thermal noise is capable of triggering the array more frequently, and the rate responds *exponentially*.

4.3 ANITA and its Trigger

The ANITA experiment has a multi-staged trigger, and seeks to find signals that are impulsive, broadband, and have plane-wave characteristics. The four stages must produce a global trigger rate of 30 Hz. For each event, ANITA incurs about 10 ms of deadtime in digitization, and so has a maximum hardware trigger rate of 100 Hz. However, writing the data to disk cannot be accomplished faster than 30 Hz, and this sets the global trigger maximum.

We will focus on the ANITA-2 system which has a four-layer trigger, "L0", "L1", "L2", and "L3". As with ARA, the L0 is a single-channel power-based trigger. The ANITA-2 experiment split the incoming antenna signal into three non-overlapping frequency bands (200-350 MHz, 330-600 MHz, 630-1100 MHz) and a full band of 150-1240 MHz. The L0 trigger is formed when any band has a integrated power level of 3.7 times the mean noise power in a few-nanosecond window [30], enforcing the impulsive nature of the Askaryan radiation. The integration is done with diodes as in ARA [1], and the math for the single-band trigger rate is identical to that of single-channel trigger rate in ARA via equation 3. A plot of the Anita-2 L0 (and L1) trigger rates as a function of power over average power is given in figure 6. The 3.7 P_{rms} diode threshold corresponds to a single-band trigger rate of anywhere from 1 MHz in the full band to 14 MHz in the 200-350 MHz band for ANITA-2 [22]. As with ARA, the trigger threshold is continually adjusted throughout the flight.

[1] In fact, the ANITA experiment actually used them first, and ARA inherited them.

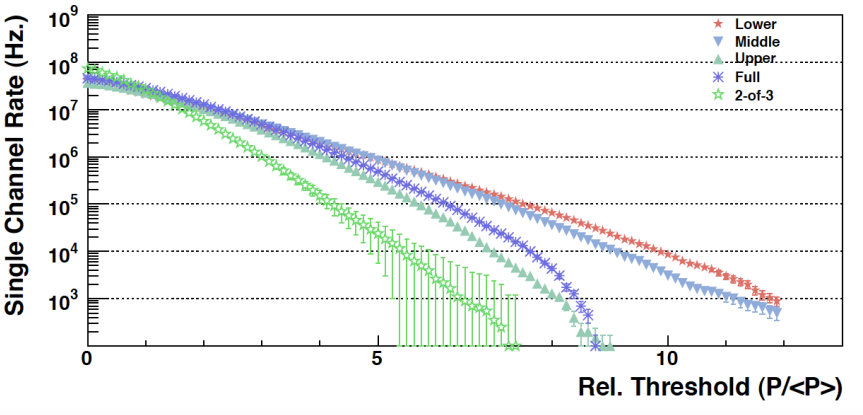

Figure 6: The dependence of the ANITA-2 L0 and L1 single-channel trigger rates on the trigger threshold, which is the ratio of power to average power. Figure by R. Nichol from [33]. "Lower" means the lower frequency band (200-350 MHz), "middle" means the middle frequency band (330-600 MHz), and "upper" means the highest frequency band (630-1100 MHz). "Full" indicates the full band, and "2-of-3" indicates the L1 trigger rate of 2/3 sub-band coincidence.

An L1 trigger is formed when 2/3 split bands and the full band all obtain an L0 trigger within a 10 ns coincidence window. The L1 trigger is a way of insisting on a broadband signal. The triggering math for a single antenna is therefore the same as found in ARA equation 4 save the factor of 2. $R_{L1} = \frac{8!}{(3!\cdot 8!)} r_{L0}^3 \tau^2$ for $r_{L0} = 1$ MHz and $\tau_{L1} = 10$ ns gives $R_{L1} = 179.2$ kHz [34]. The observed rate of L1 triggers in ANITA-2 is $\sim$ 200 kHz for the top and middle rings of antennas, which is close to the theoretical prediction [22]; the rate is $\sim$ 800 Hz for the bottom ring, which is intentionally lower (see below).

In the top and middle ring, an L2 trigger is formed when any 2 of a group of 3 adjacent antennas have an L1 trigger in a 20 ns window; the rate for L2 is then $R_{L2,top/middle} = \frac{3!}{(2!\cdot 1!)} r_{L1}^2 \tau_{L2}$ where $r_{L1} = 200$ kHz as derived above, and $\tau_{L2} = 20$ ns, giving $R_{L2,top/middle} = 2.4$ kHz. The experimentally observed L2 rate is $\sim$ 3 kHz [22]. For the bottom ring, the L2 trigger only required an L1 trigger in an adjacent antenna; this is a looser requirement than for the top and middle rings. This was necessary in ANITA-2 because there were fewer antennas in the bottom ring; the bottom ring thresholds are tuned to produce L1 rates of 800 Hz so that the total number of global triggers per antenna was roughly constant.

The L3 trigger, or "global" trigger for ANITA-2 is formed by requiring two of three rings have an L2 trigger in a 30 ns window. The L2 and L3 triggers combined assert that at least four antennas must trigger, which is enough to localize the plane of arrival for the signal. There are three cases

Experiment	Trigger Summary	Deadtime Per Event
IceCube	0.25 Single-Photoelectrons Per DOM, 5 Nearest Neighbor DOMs with signal in 2 μs window	26 μs
ARA	Power above threshold in 3/8 antennas in 170 ns window	21 ms
ANITA-2	Power above threshold in 3/4 triggering bands per antenna in 10 ns window, for 2/3 adjacent antennas in 20 ns window, in at least two rings in 30 ns window	20 ms

Table 1: A summary of the triggering conditions and their associated deadtimes for the three experiments considered.

for the L3 trigger: top+middle, top+bottom, and middle+bottom. However, the small triggering rate for the bottom ring means the global trigger rate is dominated by coincidences between the top and middle ring. So the theoretical global L3 trigger occurs at a rate approximately given by $R_{L3} = 16 \cdot R_{L2,top} \cdot R_{L2,middle} \cdot \tau_{L3}$ which for $R_{L2,top/middle} = 2.4$ kHz and $\tau_{L3} = 30$ ns gives $R_{L3} \approx 3$ Hz. The experimentally observed rate is 10 Hz [22] within a factor of three of the estimate.

In summary, the global trigger rate depends exponentially on the single-band trigger threshold: $R_{global} \propto e^{-3P_{th}}$. We note that parameters such as the timing windows in the coincidence triggers are *physically motivated*; for example, 30 ns is chosen as the L3 time window to allow a light signal to causally traverse the 5 meter height of the array. This underscores the interplay between the trigger and the hardware construction, and emphasizes the importance of the trigger's optimization.

5 How the Trigger Threshold Affects Experimental Sensitivity

The trigger threshold has direct connections to the physics and astronomy probed by the experiments. Decreasing thresholds will result in lower energy thresholds, larger apertures, and improved efficiency for signal detection, though all at the expense of higher event rates.

5.1 Trigger Effects on the IceCube Energy Threshold

In IceCube, the trigger threshold directly controls the energy threshold by setting the minimum length of a detected track. The length of the track is controlled by the energy loss of charged particles in matter and is encoded in the number of Cherenkov photon receiving DOMs. For purposes of the threshold calculation in IceCube, we focus on muons and their tracks; this is also illustrative as muons are the principal background. Muons, as massive charged particles,

are capable of losing energy through four key processes besides Cherenkov radiation: ionization, electron-positron pair production, bremsstrahlung, and photonuclear losses [35]. The rate of muon energy loss per unit length dE/dx due to all of the factors can be parametrized succinctly as [35]:

$$\frac{dE}{dx} = -a(E) - b(E)E \tag{5}$$

where $a(E)$ represents the ionization energy loss and is given by the classical Bethe-Bloch equation [12], while $b(E)$ captures all of the effects of electron-positron pair production, bremsstrahlung, and photonuclear interactions. Ionization losses are relatively constant at $a(E) \approx 0.2$ GeV/m (in ice) for muons between 100 Mev and several hundred GeV. Once activated, the latter three loss effects are also roughly a constant at $b(E) = 4.2 \times 10^{-4}$/m [36]. They become dominant at the "critical energy," defined as $E_{critical} = a/b$ [35] which for a muon in ice is about 500 GeV. Solving[2] equation 5 gives the track length estimate as a function of muon energy E_0:

$$L \approx \frac{1}{b} \ln\left(1 + \frac{E_0 b}{a}\right) = 2380\text{m} \cdot \ln\left(1 + \frac{E_0(\text{GeV})}{500\,\text{GeV}}\right) \tag{6}$$

In practice the track length is determined by the number of DOMs that collect Cherenkov photons. The Cherenkov emission received in the DOMs follows the Frank-Tamm formula [11] which states that the number of photons emitted per unit length the muon traverses, per wavelength of photon emitted is given by:

$$\frac{d^2N}{dxd\lambda} = \frac{2\pi\alpha z^2}{\lambda^2}\left(1 - \frac{1}{\beta^2 n^2}\right) \Longrightarrow \frac{dN}{dx} = \int_{300\,\text{nm}}^{650\,\text{nm}} \frac{d^2N}{dxd\lambda} d\lambda = 823 \sin^2\theta_c \ \frac{\text{photons}}{\text{cm}} = 528 \ \frac{\text{photons}}{\text{cm}} \tag{7}$$

where $\alpha = 1/137$ is the fine-structure constant, $\beta = v/c$, n is the index of refraction, and z is the atomic number of the medium. In the last equality we integrated over the IceCube wavelengths of interest (300-650 nm) and assumed the lower-limit of $z = 1$ (vacuum). Note that the Cherenkov emission does not depend on the energy of the muon so long as the particle is above the Cherenkov emission threshold of 20 MeV.

[2] $E(L, E_0) = \left(E_0 + \frac{a}{b}\right)\exp(-b \cdot L) - \frac{a}{b}$

Once the length of the track has been estimated by counting the number of DOMs with a signal, we can utilize equation 6 to estimate the energy. The 5-LC trigger currently used in IC-86 could be satisfied by a completely vertical track which must then traverse $5 \cdot 17$ meters = 85 meters total. Then, inverting equation 6 we find $E_{min,5LC} = \left(\exp\left(\frac{85\text{m}}{2380\text{m}}\right) - 1 \right) 500\,\text{GeV} = 18$ GeV, or a 40 GeV neutrino. The collaboration estimated that <TeV muons travel about 5 m per GeV in ice [25], and so the spacing of the bulk DOMs (17 m vertically and 125 between strings) limits them to events between 50 GeV and 100 GeV. The published sensitivity of the bulk detector is 100 GeV [16], in good agreement with these estimates. In DeepCore, where the spacing is reduced to 10 meters between DOMs and the LC trigger threshold reduced to three-nearest-neighbor DOMs (at its weakest), the energy thresholds plummets another factor of three to 6.4 GeV, or an approximately 12 GeV neutrino. The quoted energy sensitivity for IceCube DeepCore is indeed 10 GeV [25]. The DOM LC requirement impacts the physics reach of the experiment, as tuning the LC requirement controls the accessible energies of the array. Decreasing the DOM spacing and relaxing the LC trigger gives access to lower energy events. In fact, because the track length depends logarithmically on the shower energy, there is an *exponential* dependence of the neutrino energy on the track length.

The decision to use a tunable LC trigger also had design implications for IceCube. To enable rapid DOM communication, all DOMs are connected by dedicated twisted-wire pairs to their nearest-neighbor same-string DOMs [15]. As the DOMs cannot be recovered from the ice and the communications feed added in after the fact, careful studies and simulations of the DOM trigger must have directly informed the final design decision to include the dedicated channels. The trigger scheme and threshold had direct consequences for the design of the detector.

5.2 Trigger Effects on the ANITA and ARA Sensitivity

5.2.1 Energy Threshold

Because the single-antenna / single-band trigger forms the base of the global trigger, the energy threshold of the ANITA and ARA experiments are in fact set *exclusively* by the energy threshold of single antennas. An effective way of parametrizing this connection is through the signal to noise ratio or SNR. The SNR characterizes how much larger a "signal" is than the ambient noise background. We define an event's SNR as $SNR = V_{signal}/V_{rms}$, where V_{rms} is the voltage level in

the antenna induced by thermal noise radio waves in equation 2.

V_{signal} is induced in the antenna by the electric fields from the EM and hadronic cascades of neutrino-nucleon interactions. The magnitude of the Fourier transform of the field $|\tilde{\mathbf{E}}|$ can be obtained in the far field by the following parametrization by Jaime Alvarez-Muniz [37]. The equation is a fit to Monte Carlo simulations, and its high fidelity has been verified extensively, for example, Hanson *et. al.* [38].

$$\frac{|\tilde{\mathbf{E}}(f,R,\theta)|}{\left[\frac{\mathrm{V}}{\mathrm{MHz\cdot m}}\right]} = 1.1\times10^{-7}\left[\frac{E_0}{1\,\mathrm{TeV}}\right]\left[\frac{f}{f_0}\right]\left[\frac{1}{1+(f/f_0)^{1.44}}\right]\exp\left[-\frac{1}{2}\left(\frac{\theta-\theta_c}{2.2}\frac{f}{1\mathrm{GHz}}\right)^2\right]\left[\frac{1}{R}\right] \quad (8)$$

E_0 is the energy of the EM or hadronic shower in TeV, f is the frequency of a given mode in MHz, R is the scalar distance from the observation point to the shower in meters, $f_0 = 1150$ MHz, θ_c is the Cherenkov angle, and θ is the viewing angle. The exponential term sets the profile of the cone width, showing that the intensity of the field is strongly peaked at the Cherenkov angle, and falls off as a Lorentzian as the signal is viewed increasingly "off-cone". It is from this exponential term that we deduce the angular width of the shower to be $< 6^\circ$ in width. The field falls off as $1/R$ as is true of all classical radiation fields.

The signal propagates to the antenna, and the voltage received across some resistance load is given by equation 9 from reference [19, 29] as:

$$\tilde{V}(f) = \frac{|\tilde{\mathbf{E}}(f,R,\theta)|\cdot\tilde{h}_{eff}(f)}{2}\ \frac{\mathrm{V}}{\mathrm{MHz}} = \frac{|\tilde{\mathbf{E}}(f,R,\theta)|}{2}\cdot 2\sqrt{\frac{ZGc^2}{4\pi n f^2\eta}}\ \frac{\mathrm{V}}{\mathrm{MHz}} \quad (9)$$

where we have inserted $\tilde{h}_{eff}(f)$ in the last equality. $\tilde{h}_{eff}(f)$ represents the effective height of the antenna in frequency space. It incorporates the radiation impedance Z, the impedance of free space $\eta = 377\,\Omega$, the index of refraction of the medium in which the antenna is placed n, and the gain of the antenna G.

To determine the physical voltage received at an antenna we Fourier transform equation 9 to obtain equation 10

$$V(t) = \int_{-\infty}^{\infty}\tilde{V}(f)\,e^{\pm i2\pi ft}\,df\ \ \mathrm{Volts}\ \ \leq \int_{-\infty}^{\infty}\tilde{V}(f)\,df\ \ \mathrm{Volts} \quad (10)$$

Parameter	**ARA Value**	**ANITA Value**
System Temperature (T, Kelvin)	325 K	325 K
Bandwidth (Δf)	650 MHz	1000 MHz
Thermal Noise Voltage ($V_{rms} = \sqrt{4k_B T \Delta f Z}$, μV)	24 μV	29 μV
Distance To Event (R, km)	2 km	600 km
Index of Refraction Around Antenna (n)	1.78	1.0
Antenna Impedance (Z, Ω)	50 Ω	50 Ω
Antenna Gain (G, dBi)	1 dBi	10 dBi
Degrees off cone ($\lvert\theta - \theta_c\rvert$)	1°	1°
Neutrino Energy (E_ν, eV)	$2{\times}10^{16}$ eV	$2{\times}10^{18}$ eV
Shower Energy ($E_0 = 0.2 \cdot E_\nu$, eV)	$4{\times}10^{15}$ eV	$4{\times}10^{17}$ eV
Voltage at Antenna ($V(t)$ equ 10, μV)	29 μV	40 μV
Signal-to-Noise Ratio (SNR, $\mathbf{V(t)/V_{rms}}$)	**1.2**	**1.4**

Table 2: A calculation of the signal-to-noise ratio for ARA and ANITA that demonstrates the rough energy thresholds of the experiments.

An upper limit on the signal strength can be derived by assuming a stationary phase factor of unity in the integral, i.e. $e^{\pm i2\pi ft} \to 1$ as in the last inequality.

First-order approximations of the energy thresholds for ARA and ANITA can be determined by asking for SNR ≥ 1. The calculation is performed and summarized in table 2. From it, we deduce the energy thresholds for ARA and ANITA to be roughly 10^{16} eV and 10^{18} eV respectively. Had we assumed an EM shower for the neutrino-induced cascade, our E_0 would have been a factor of four larger, given $E_{0,EM} = 0.8 \cdot E_\nu$ while $E_{0,hadronic} = 0.2 \cdot E_\nu$. As such, *at threshold, both ANITA and ARA are more sensitive to electron neutrinos*, as this lepton flavor most easily induces EM cascades.

The trigger threshold has direct influence on the energy threshold, range, and effective volumes of the detector. Because $V_{th} \propto |\tilde{\mathbf{E}}(f, R, \theta)| \propto E_\nu$, lowering V_{th} corresponds *linearly* to accessing lower energy neutrinos. For a fixed SNR$>$ 1, and therefore a fixed efficiency for detecting a pulse, lowering the V_{th} by a factor of two allows access to neutrinos half as energetic. Further, because $V_{th} \propto 1/R$, lowering thresholds *directly* enhances sensitive to events from further away. For example, reducing thresholds by a factor of 2 enables sensitivity to events from twice as far away. This alone explains the almost 2 orders of magnitude difference in the ARA and ANITA energy thresholds; ARA as an *in-situ* experiment can access weaker electric-fields over the same thermal noise background. The apertures are also affected because to first-order the ice volume to

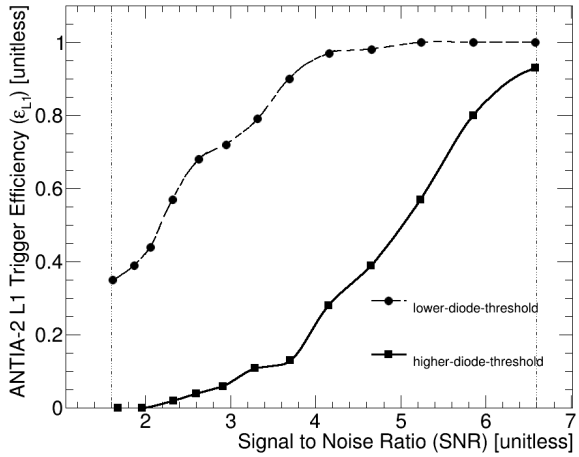

Figure 7: The efficiency $\mathcal{E}_{L1}$ for pulse detection in the ANITA-2 L1 trigger as a function of SNR for two different diode thresholds. The vertical bars mark where measurements stopped. Data from [39].

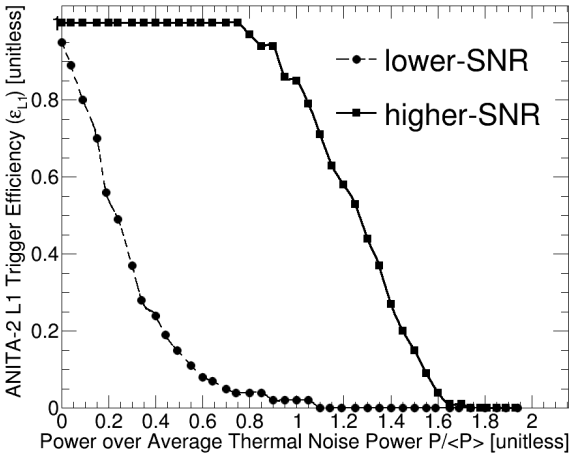

Figure 8: The efficiency $\mathcal{E}_{L1}$ for pulse detection in the ANITA-2 L1 trigger as a function of power over mean thermal noise power, otherwise known as the diode threshold setting. Data from [39].

which an antenna has access goes as R^3. So for fixed SNR the same factor of 2 which yields events from twice as far away has the potential to increase the effective volume by a factor of *8*. This implies a cubic (quadratic) dependence the effective volume (area). There is another enhancement to the effective volume that is associated with the shape of the Cherenkov cone. Recall that the Askaryan pulse is weaker in magnitude and broader in time as it is viewed increasingly off cone (see fig 2). Therefore, the ability to detect weaker signals means the antennas are capable of detecting the pulse further off cone. This allows for a larger set of interaction points in the ice that generate detectable signals once propagated to the antenna, and therefore increases in the effective volume.

5.2.2 Signal Detection Efficiency

The triggering schemes are not perfect at identifying signals; for a given input pulse SNR they have some *efficiency* ($\mathcal{E}$) for actually triggering on a pulse when it is present. A common parametrization of this efficiency is obtained by finding the efficiency surface for pulse detection as a function of SNR and trigger thresholds: $\mathcal{E}_{L1}(SNR, V_{th})$. In practice, this is found empirically by firing pulses of known SNR into the signal chain, and recording what fraction of pulses pass the trigger for a given threshold. One can view 1-D projections of this surface by plotting $\mathcal{E}_{L1}$ vs SNR for a given threshold as in figure 7, or by plotting $\mathcal{E}_{L1}$ vs threshold for a given SNR as in figure 8.

The curves are qualitatively intuitive. As is clear in figure 7, lower thresholds correspond with efficiency curves that "turn-on" faster; the experiment is capable of seeing "smaller" signals. Likewise, in figure 8 for higher SNRs, the efficiency curves "turn-off" more slowly; the experiment can see the "big" signals even with higher noise power threshold. The triggering efficiency can also be determined for the global trigger, and is given in figure 9 for the ANITA-2 experiment and for the ARA Testbed. The ANITA-2 experiment reaches 50% efficiency at SNR = 3.23 and is fully saturated by an SNR of 5. The ARA prototype, whose triggering scheme is similar to that of the full stations reaches 50% efficiency at an SNR = 3.5 and is fully saturated by SNR = 4. The goal of the experiment is to push the 50%-point of the efficiency curve as close to zero as possible so as to remain sensitive to the weakest signals possible. This allows access to the lowest energy events and events from the furthest distances.

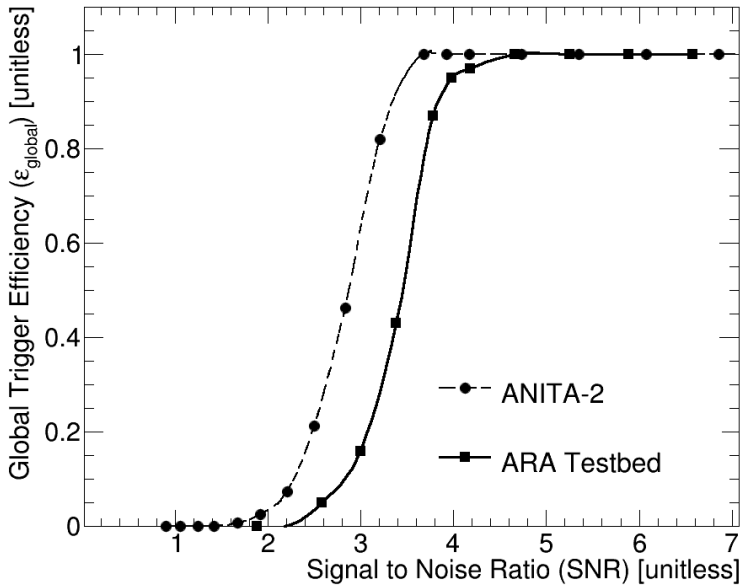

Figure 9: The efficiency $\mathcal{E}_{global}$ for pulse detection in the ANITA-2 and ARA Testbed global triggers as a function of SNR. ARA curve from [8] and ANITA-2 curve from [33].

6 Optimizing a Trigger

With the enormous advantages gained in sensitivities from lowering thresholds, the ANITA and ARA experiments constantly seek to minimize it. Constraining this desire to suppress thresholds ever closer to zero is the aforementioned hardware maximum trigger rate. This can be thought of

as two competing effects: a need to stay under a hardware maximum rate, which drives thresholds high and rates low, and a desire to access weak signals, which drives thresholds low and event rates high. Given these two hard rails, the experiments attempt to create triggers that *minimize* the 50%-point of the $\mathcal{E}_{global}$ vs SNR curve (fig 9) while *maximizing* the effective areas/volumes of the experiments.

There are several ways to achieve the minimization of this global-efficiency-50%-point. Take for example the case of ARA, where there are in fact *3* thresholds in R_{global} in equation 4–there is R_{L0}, but also τ the time window for coincidence, and the decision to require 3/8 antennas. A reduction in the trigger time window or a reduction in the number of antennas required would allow ARA to tolerate a higher R_{L0} and a correspondingly lower V_{th}. The dimensionality of the space is larger for ANITA; the four stage triggering scheme has at least seven adjustable parameters: the L0 power threshold V_{th}, the number of bands, antennas, or rings required in the L1, L2, and L3 triggers, and the corresponding trigger windows τ_{L1}, τ_{L2}, and τ_{L3}.

The constraint to maximize the effective area is less straightforward to implement; we expect effective area maximization would suppress the trigger threshold due to the cubic (quadratic) growth of the effective volume (area) as V_{th} is reduced, but this fails to account for other effects like ice attenuation, which we earlier ignored in our first-order approximations. Such effects may render the threshold suppression moot. Even so, there are ways to at least constrain the parameter space. τ_{L3} for ANITA should allow a plane wave to traverse the 5m height of the array. The SNR should be greater than 1. Insight from post-processing analysis can be consulted; in ARA's case, running analysis algorithms on simulations with less than 3 triggering antennas exhibited poor event reconstructability [40]. If a detector has had success with identifying signal events (like ANITA-1 and ANITA-2 had with cosmic rays) these old events can be examined for passability under the new trigger. In an ideal situation, an experimentalist should choose a set of trigger constraints, simulate the full experiment, and compute the effective volume/threshold for every candidate trigger configuration. We have found very little literature to this effect despite the effective volume being the other key parameter for detector sensitivity aside from the energy threshold. We suspect this is due to the time and computational-resource intensive task of generating such a large ensemble of simulations.

The IceCube experiment is not exempt from this "race to zero threshold" syndrome; it seeks to lower the number of DOMs in the LC trigger to access shorter tracks and therefore lower energy physics. Indeed, this was the design principle behind the DeepCore infill array. But weaker LC-coincidence requirements mean commensurately more events. As such, IceCube must also balance the desire to implement very low thresholds against a hardware maximum. In determining the optimum trigger for IceCube, difficulties arise from determining in what *directions* should the LC coincidence requirement be satisfied for, and the number of DOMs in the LC coincidence. Requiring a twenty-DOM-vertical trigger would impose the same track length constraint as a three nearest-neighbor-*string* requirement, but the latter is much more sensitive to earth-skimming neutrinos, where the former prefers vertical tracks. Note that nearest-neighbor-string hardware is not currently implemented, but could be developed. So if the experiment is tuning for sensitivity to PeV neutrinos and above, exploring the nearest-neighbor-*string* trigger might be productive. Such triggering schemes have been explored as ways to enhance sensitivity to certain physics; dark matter annihilation to muons from the center of the earth is expected to produce upgoing, vertical tracks, for example[41]. *The broader the physics mission, the more general the trigger, and the more voluminous the data for post-trigger processing.* Consider figure 3 right; if IceCube's sole mission was detection of cosmogenic neutrinos, they could simply impose a 400 DOM trigger; but their desire to do other physics, like probe the flux of atmospheric neutrinos, forces them to hold the LC condition lower.

We conclude this section by suggesting a generic trigger optimization procedure; we will make these steps concrete with examples from ARA.

1. Create figures of merit by which to evaluate the trigger; the trigger will be optimized by demanding the minimization or the maximization of these figures of merit. EX: ARA might desire to minimize the 50%-SNR-efficiency point or maximize the effective volume.

2. Identify all input parameters to the trigger and their constraints. These are the inputs to the trigger, and will be varied to determine the optimum trigger configuration. EX: A parameter for ARA is the coincidence time window; it is constrained by a need to be large enough to allow a plane wave to traverse the array.

3. Identify the maximum trigger rate. EX: ARA has data storage limitations, and cannot trigger faster than 5 Hz.

4. Obtain and implement the trigger in a simulation of the full experiment. EX: For ARA, the simulation software package is AraSim.

5. Run the simulation over every possible combination of parameters, with the constraint that a given combination of parameters does not violate the hardware maximum trigger rate described in step 3. EX: In ARA, we could test a time window of 100, 150, ... ns. For each time window possibility, we could try triggering on 1, 2, 3, ... 8 antennas. For each combination of time window and antenna trigger number, we can test triggering on power thresholds of 1, 2, 3, ... times the average thermal noise power. Only run simulations for combinations of parameters that keep the global trigger threshold under the maximum identified in step 3. (Aside: the need to run many simulation as part of a trigger optimization is one of the principal reasons to develop fast simulations tools.)

6. From all of the output generated by step 5, identify the combination of parameters that maximizes or minimizes your chosen figure of merit. EX: In ARA, we may choose the combination which maximizes the effective volume.

7 Future Prospects: A Phased Array Concept

Phased array techniques can lower energy thresholds and enhance physics sensitivity for ground-based antenna arrays like ARA, potentially allowing for sensitivity overlap with the IceCube experiment. The proposed project accomplishes this by enhancing this SNR through background reduction. This can be accomplished with signal averaging methods, where averaging over many waveforms of the same signal generates a growth in the signal as n (the number of waveforms), but only enlarges the noise by a factor of $\sqrt{n}$, and so the SNR on the whole grows as $n/\sqrt{n} = \sqrt{n}$. For the single-channel transient triggers in ANITA and ARA, this is impossible; they only ever have one sample of the data that can be considered. A recently proposed *in-situ* neutrino phased array project named the Greenland Neutrino Observatory (GNO) by Vieregg *et al.* [42, 43] intends to solve this problem by combining the waveforms from multiple antennas before making the trigger decision. This would achieve the $\sqrt{n}$ enhancement in the SNR and enable signal observation from events that are a $\sqrt{n}$ lower in energy, or from $\sqrt{n}$ further away, or enhance the effective volume (area) by $n^{3/2}$ (n), in addition to the off-cone viewing capability.

To average down the backgrounds the waveforms must be added coherently. For a plane wave striking a string of antennas from a given incoming direction, each antenna would record the signal pulse (time delayed relative to one another) and the noise environment. The sum of those waveforms, corrected for travel time between antennas (this is known as the *coherent sum*), will see the incoherent noise average to zero while enhancing the signal. That set of time delays is unique to that direction of arrival; by varying the time delays differently, the coherent sum becomes sensitive

to signals coming from an entirely different direction. This technique of varying time delays to tune sensitivity to different signal directions is known as *beamforming*. Beamforming is an effective way to boost the gain of the antennas; Vieregg [42] identifies that the effective gain of this beam as

$$G_{eff} = 10 \cdot \log_{10}\left(N \times 10^{G/10}\right) \tag{11}$$

where N is the number of antennas in the beam and G is the gain of the individual antennas. Phasing enhances the effective gain of ground-based arrays like ARA, which are typically constrained to low-gain antennas because of the need to fit them down the small cylindrical boreholes in the Antarctic ice and maintain the antenna's azimuthal symmetry.

The principal advantage of the phased array is reduced thresholds. Recall from equation 9 that the input voltage to an antenna $V \propto E \cdot h_{eff} \propto E \cdot \sqrt{G}$. The aforementioned $\sqrt{n}$ enhancement of the electric field allows GNO to lower V_{th} by the same factor. By utilizing sixteen antennas for example, GNO can detect neutrinos with a quarter as much energy, or events that arrive from four times as far away than its unphased counterpart. The gain factors of these phased antennas rapidly approach that of standard directional antennas; sixteen antennas of 2.15 dBi each have an effective gain of 14.2 dBi, already greater than the ANITA peak-gain of 10 dBi. Early measurements [43] of a toy-model of the phased array in an anechoic chamber shows that even for the simple case of three antennas, the 50%-efficiency point for pulse detection occurs for an SNR of 2. This is nearly half the present ARA 50%-efficiency point of 3.5, underscoring the potential advantage of an array such as GNO. The advantages only become more dramatic as the number of antennas is scaled up; for an ideal array of 400 antennas, the electric field threshold is reduced by a factor of 20, pushing the threshold energy of the array to 10 PeV and below. This means GNO would have the physics capability to perform direct cross checks of the measured PeV flux by IceCube. A secondary advantage is the ability to, in real time, avoid forming beams in directions of the sky which are noisy. This ability to turn off loud beams allows the array to continue riding the thermal noise. At an advanced stage, GNO could potentially steer the beams in real-time to focus sensitivity in the direction of sources identified by the early warning systems in place for GRBs, supernovae, etc.

The array has a number of engineering and design challenges. Principle amongst these is a need for many beams to blanket the ice of interest; by combining beams pointing in many different

directions, one can achieve comparable coverage to an omni-directional antenna trigger [42]. But finite beam width and beam numbers means the array will have to choose which portions of the sky to watch and which to ignore. The beamforming must also be done on the timescales of microseconds, and poses a challenge to the firmware and FPGA (field programmable gate array), as the number of permutations needed to phase together all of the channels grows with the number of antennas. The placement of many antennas down holes in a densely packed fashion is challenging; GNO will only be able to place so many before the hole runs out of depth, and then it must start drilling other lateral holes, driving up the expense of the project and complicating the beamforming calculation. Lastly, the antennas cannot be packed so densely that the detected noise in the two becomes correlated. Measurements were made of candidate antennas (the same as the ARA antennas) in an anechoic chamber [43] and demonstrate that coherence effects are not detectable for any achievable antenna configuration. Measuring correlated noise would require the antennas be more closely packed together than is physically possible.

In summary, the GNO experiment is a very promising avenue for reducing the energy threshold of the ground based radio neutrino telescopes yet again and finally offer cross checks of the IceCube PeV neutrino spectrum. The project has formidable engineering challenges, but the collaboration is optimistic about their ability to conquer them, and initial work [43] suggests they will succeed.

8 Acknowledgments

I would like to thank my advisor Prof. Amy Connolly and her research group here at OSU. I thank Prof. Connolly for her extraordinary support and mentorship throughout my graduate research career so far. In the Connolly group, I give special thanks to graduate student Oindree Banerjee for supporting me throughout my candidacy, and offering many insightful comments and discussions. I would also like to thank postdoctoral researchers Dr. Jordan Hanson, Dr. Carl Pfendner, Dr. Michael Sutherland, and research scientist Dr. Patrick Allison for valuable advice on various experiments. Special thanks are due to Dr. Hanson for many helpful conversations about the Askaryan signal and the philosophy of trigger design. Thanks to Dr. Pfendner, Dr. Hanson, and Oindree for helpful comments on drafts of this paper.

Enormous thanks to my parents Vann and Cindy Clark for their life-long support of my love of learning, and also to my high school Physics teacher Erin Mulanax, without whom I never would have discovered the joys of physics. Thanks also to my physics cohort, particularly Humberto Gilmer, Kathryn Nicolich, Kasandara Sullivan, and Tony Lefeld for moral support during my first two years and the candidacy process.

This work is made possible by generous funding from many organizations. I am especially thankful for support from the NSF GRFP (Award DGE-1343012). I would also like to thank the OSU Physics and Astronomy Departments, as well as the OSU Graduate School, for Fellowship and Teaching Associateship Support during my first two years.

References

[1] The IceCube Collaboration. IceCube Preliminary Design Document. 2001.

[2] Eli Waxman and John N. Bahcall. High-energy neutrinos from cosmological gamma-ray burst fireballs. Phys. Rev. Lett., 78:2292–2295, 1997.

[3] G. T. Zatsepin and V. A. Kuz'min. Upper Limit of the Spectrum of Cosmic Rays. Soviet Journal of Experimental and Theoretical Physics Letters, 4:78, August 1966.

[4] K. Greisen. End to the Cosmic-Ray Spectrum? Physical Review Letters, 16:748–750, April 1966.

[5] V. S. Beresinsky and G. T. Zatsepin. Cosmic rays at ultra high energies (neutrino?). Physics Letters B, 28:423–424, January 1969.

[6] M. Ahlers, L. A. Anchordoqui, M. C. Gonzalez-Garcia, F. Halzen, and S. Sarkar. GZK Neutrinos after the Fermi-LAT Diffuse Photon Flux Measurement. Astropart. Phys., 34:106–115, 2010.

[7] Amy Connolly, Robert S. Thorne, and David Waters. Calculation of High Energy Neutrino-Nucleon Cross Sections and Uncertainties Using the MSTW Parton Distribution Functions and Implications for Future Experiments. Phys. Rev. D, D83:113009, 2011.

[8] Anita Collaboration and P. W. Gorham. The Antarctic Impulsive Transient Antenna ultra-high energy neutrino detector: Design, performance, and sensitivity for the 2006-2007 balloon flight. Astroparticle Physics, 32:10–41, August 2009.

[9] M. C. Gonzalez-Garcia, Francis Halzen, and Soumya Mohapatra. Identifying Galactic PeVatrons with Neutrinos. Astropart. Phys., 31:437–444, 2009.

[10] P. Allison et al. First Constraints on the Ultra-High Energy Neutrino Flux from a Prototype Station of the Askaryan Radio Array. Astropart. Phys., 70:62–80, 2015.

[11] John David Jackson. Classical Electrodynamics. 1999.

[12] K. A. Olive et al. Review of Particle Physics. Chin. Phys., C38:090001, 2014.

[13] R. Abbasi and et al. Calibration and characterization of the IceCube photomultiplier tube. Nuclear Instruments and Methods in Physics Research A, 618:139–152, June 2010.

[14] M. Ackermann and et al. Optical properties of deep glacial ice at the South Pole. Journal of Geophysical Research (Atmospheres), 111(D10):D13203, July 2006.

[15] R. Abbasi, M. Ackermann, J. Adams, M. Ahlers, J. Ahrens, K. Andeen, J. Auffenberg, X. Bai, M. Baker, S. W. Barwick, and et al. The IceCube data acquisition system: Signal capture, digitization, and timestamping. Nuclear Instruments and Methods in Physics Research A, 601:294–316, April 2009.

[16] Francis Halzen and Spencer R. Klein. Invited review article: Icecube: An instrument for neutrino astronomy. Review of Scientific Instruments, 81(8), 2010.

[17] Askaryan G. A. Excess Negative Charge of an Electron-Photon Shower and its Coherent Radio Emission. Soviet Physics JETP, 14(2), February 1962.

[18] P. W. Gorham, D. P. Saltzberg, P. Schoessow, W. Gai, J. G. Power, R. Konecny, and M. E. Conde. Radio-frequency measurements of coherent transition and Cherenkov radiation: Implications for high-energy neutrino detection. Physical Review E, 62:8590–8605, December 2000.

[19] P. Miočinović, R. C. Field, P. W. Gorham, E. Guillian, R. Milinčić, D. Saltzberg, D. Walz, and D. Williams. Time-domain measurement of broadband coherent Cherenkov radiation. Physical Review D, 74(4):043002, August 2006.

[20] A. M. Jaime, A. Romero-Wolf, and E. Zas. Time domain radio pulses from particle showers. Nucl Instr and Methods A, 662:S32–S5, 2012.

[21] ANITA Collaboration. ANITA: A Concept Study Report to the NASA Small Explorers Program. 2004.

[22] Abigail Vieregg. The Search For Astrophysical Ultra-High Energy Neutrinos Usgin Radio Detection Techniques. Doctoral Thesis, University of of California Los Angeles, 2010.

[23] ARA Collaboration and P. Allison. Design and initial performance of the Askaryan Radio Array prototype EeV neutrino detector at the South Pole. Astroparticle Physics, 35:457–477, February 2012.

[24] IceCube Collaboration. 2008 IceCube Update. 2008.

[25] R. Abbasi and The IceCube Collaboration. The design and performance of IceCube DeepCore. Astroparticle Physics, 35:615–624, May 2012.

[26] Michelangelo D'Agostino. First Evidence for Atmospheric Neutrino-Induced Cascades with the IceCube Detector. 2009.

[27] J. Ahrens and The IceCube Collaboration. Sensitivity of the IceCube detector to astrophysical sources of high energy muon neutrinos. Astroparticle Physics, 20:507–532, February 2004.

[28] P Allison. private communication, 2016.

[29] Eugene Hong. Searching for Ultra-high Energy Neutrinos with Data from a Prototype Station of the Askaryan Radio Array. Doctoral Thesis, The Ohio State University, 2014.

[30] Amy et al Connolly. Thermal Nosie Studies, Toward a Time-Domain Model of the ANITA Trigger. ANITA Collaboration E-Log Entry, 2006.

[31] Ming-Yuan Lu. Trigger Window Optimization Studies. ARA Collaboration Internal Note, docDB 928-v1, 2014.

[32] Thomas Mueres. Development of a Sub-glacial Radio Telescope for the Detection of GZK Neutrinos. Doctoral Thesis, University Libre Brussels, 2015.

[33] Matthew Mottram. A Search for Ultra high Energy Neutrinos and Cosmic-Rays with ANITA 2. Doctoral Thesis, University College London, 2012.

[34] G. S. Varner, P. W. Gorham, A. Jongeling, and L. A. White. The ANITA Trigger Logic: Estimates of t Thermal Noise Trigger Rates and Practical Operating Thresholds. ANITA Note 04-022, 2004.

[35] Bressieux Joseph. Testing and Comparison of muon energy estimators for the IceCube neutrino observatory. Masters Thesis, The University of Wisconsin and Ecole Polytechnique Federale De Lausanne, 2008.

[36] Chirkin D. and Rhode W. Muon Monte Carlo: A high-precision tool for muon propagation through matter. 2004.

[37] J. Alvarez-Muniz, R. A. Vazquez, and E. Zas. Calculation methods for radio pulses from high-energy showers. Phys. Rev. D, D62:063001, 2000.

[38] Jordan C. Hanson and Amy L. Connolly. Complex Analysis of Askaryan Radiation: A Fully Analytic Treatment including the LPM effect and Cascade Form Factor. 2016.

[39] Ryan Nichols. Trigger Studies. ANITA Phone Call Presentation, 2008.

[40] Ming-Yuan Lu. Station Design Study. ARA Collaboration Internal Note, docDB 1028-v3, 2014.

[41] E. Resconi and IceCube Collaboration. Status and prospects of the IceCube neutrino telescope. Nuclear Instruments and Methods in Physics Research A, 602:7–13, April 2009.

[42] A. G. Vieregg, K. Bechtol, and A. Romero-Wolf. A Technique for Detection of PeV Neutrinos Using a Phased Radio Array. JCAP, 1602(02):005, 2016.

[43] J. Avva et al. Development Toward a Ground-Based Interferometric Phased Array for Radio Detection of High Energy Neutrinos. 2016.